

Research Article

Enhancing crack detection in railway tracks through AI-optimized ultrasonic guided wave modes

Jianjun Liu^a, Huan Luo^a, Han Hu^{a,b}, Jian Li^{a,c,*}^a School of Intelligent Engineering, Shaoguan University, Shaoguan 512005, China^b Institute of Engineering Mechanics, Karlsruher Institut für Technologie, Karlsruhe 76131, Germany^c Chongqing Research Institute of HIT, Chongqing 401135, China

ARTICLE INFO

Article history:

Received 14 June 2024

Revised 3 July 2024

Accepted 19 July 2024

Available online 3 August 2024

Keywords:

Sensitivity

Crack

Guided

Modal

ABSTRACT

The utilization of ultrasonic guided wave technology for detecting cracks in railway tracks involves analyzing echo signals produced by the interaction of cracks with guided wave modes to achieve precise crack localization, which is extremely important in a real-time railway crack robotic detection system. Addressing the challenge of selecting the optimal detection mode for cracks in various regions of railway tracks, this paper presents a method for optimal crack detection mode selection. This method is based on the sensitivity of guided wave modes to cracks. By examining the frequency dispersion characteristics and mode shapes of guided wave modes, we establish indicators for crack zone energy and crack reflection intensity. Our focus is on the railhead of the railway track, selecting guided wave modes characterized by specific cracks for detection purposes. Experimental findings validate the accuracy of our proposed mode selection method in detecting cracks in railway tracks. This research not only enhances crack detection but also lays the groundwork for exploring advanced detection and localization techniques for cracks in railway tracks.

© 2024 The Author(s). Published by Elsevier B.V. on behalf of Shandong University. This is an open access article under the CC BY-NC-ND license (<http://creativecommons.org/licenses/by-nc-nd/4.0/>).

1. Introduction

The emergence of fatigue cracks and other internal damages in railway tracks can lead to rail fractures, presenting significant safety risks to railway transportation. Therefore, timely detection and precise localization of rail cracks are crucial, which is extremely important in a real-time railway crack robotic detection system. Research indicates that when ultrasonic guided waves encounter cracks, they produce reflected echoes accompanied by complex mode conversion phenomena. By gathering and analyzing the guided wave signals transmitted through transducers, it becomes possible to ascertain the presence of cracks and obtain specific information such as their location and size. Ultrasonic guided waves can effectively cover the entire cross-section of the rail, addressing the detection blind spots inherent in other non-destructive testing methods. Furthermore, these waves propagate over long distances at high speeds, ensuring efficient crack detection without disrupting train operations. Their suitability for long-distance rail crack detection is complemented by their ability to be installed on rails for continuous, all-weather monitoring, thus offering promising applications and research prospects [1,2].

However, ultrasonic guided waves possess multimodal and dispersive characteristics. In order to extract modal information from these complex signals, researchers worldwide have investigated various identification methods. These include primarily time-domain signal analysis [3], wavelet transform [4,5], Wigner-Ville distribution [6–11], two-dimensional Fourier transform [12–16], Hilbert–Huang transform [17–19], and excitation response inverse transform [20–22].

The time-domain signal analysis method determines modal velocity by calculating the arrival time of wave packets in the time-domain signal, thus identifying the modal type. This approach is well-suited for analyzing signals with simple modal components and is commonly used in research [23,24] to ascertain the presence of target modes. However, it is not suitable for analyzing complex signals with multiple modes. Amjad et al. [25] conducted time–frequency analysis on guided wave signals propagating in steel bars using the short-time Fourier transform method to identify different guided wave modes. Prasad et al. [26] applied the short-time Fourier transform method to process Lamb wave signals in composite material structures. Based on Lamb wave energy parameters, combined with iterative tomography algorithms, they reconstructed structural defects. Zhou et al. [27] analyzed the guided wave mode components inside aluminum plates using the short-time Fourier transform method and verified the presence of mode conversion phenomena through temporal changes. Feng [28] utilized the short-time Fourier transform

* Corresponding author.

E-mail address: jianli@sgu.edu.cn (J. Li).

method to analyze guided wave signals of A_0 and S_0 modes in aluminum skin honeycomb panels under both well-bonded and deboned conditions and compared the mode components under the two scenarios. However, when the frequency components of the signal are relatively complex, ensuring resolution and information integrity requires narrow time windows for high-frequency components and wide time windows for low-frequency components. Due to the fixed time window function used in the short-time Fourier transform, it is unable to simultaneously meet the time–frequency resolution requirements of both high and low-frequency components.

To address the shortcomings of the short-time Fourier transform method, researchers have introduced the wavelet transform for time–frequency analysis of ultrasonic guided wave signals. In recent years, the wavelet transform has been widely applied to modal analysis of guided wave signals in railway tracks [29–31]. Bartoli et al. [32] employed impact excitation on the railhead of railway tracks and utilized wavelet transform on the received signals to extract the vertical mode components of the guided waves. They also analyzed the influence of wavelet central frequency and shape on the modal analysis results. Lu et al. [33] conducted experimental research on the propagation characteristics of vertical vibration modes of ultrasonic guided waves in China's U60 type rails using the Gabor wavelet transform method. Liu et al. [34] identified Lamb wave modes in plates using two-dimensional Fourier transform and discussed changes in mode components of signals when Lamb waves are excited and received using straight and angled probes. Wang [35] analyzed the guided wave modes propagating in railway tracks using the two-dimensional Fourier transform method and obtained the transformation relationship between mode phase velocity and stress, demonstrating the limitations of phase velocity in railway stress detection. Xing et al. [36] proposed a single extraction algorithm for guided wave modes and applied it to crack detection in railway tracks, improving the accuracy of crack localization. This method is suitable for cases requiring high demands on mode identification. However, due to the need to collect a large amount of received signals during the detection process, the operation is relatively complex, resulting in fewer current applications.

Incorporating these advanced algorithms into self-service robot applications, the robots can be equipped to conduct real-time crack detection and maintenance on railway tracks. By utilizing ultrasonic guided wave technology and the described modal analysis methods, the robots can continuously monitor the rail conditions, detect potential cracks, and provide precise localization, thus enhancing the efficiency and safety of railway operations. This integration offers a practical application of the research, showcasing its potential in automated maintenance systems.

The aforementioned studies reveal that there are still numerous challenges to be addressed in the rail crack detection method based on ultrasonic guided waves. Due to the presence of multiple modes when ultrasonic guided waves propagate in rails, these modes exhibit certain differences, including variations in frequency, vibration patterns, and energy distribution. Different modes yield varying detection results for the same type of crack, and the detection capabilities also differ significantly for different types of cracks even within the same mode. Hence, it is crucial to analyze the mechanism of how rail cracks affect guided wave modes and to select appropriate detection modes based on different types of cracks for effective rail crack detection research.

Based on this understanding, this paper proposes an optimal detection mode selection method based on the sensitivity of guided wave modes to crack detection. Focusing on railheads as the research subject, indicators for crack zone energy and crack reflection intensity are established based on the location and trend of crack formation. This facilitates the selection of the optimal detection mode for cracks in the railhead area.

2. Evaluation method for crack sensitivity of guided wave modes

The wavelength of guided waves can significantly impact the accuracy of crack detection. Lower frequencies result in longer wavelengths, which may decrease precision in crack detection. Therefore, damage detection typically utilizes ultrasonic waves with frequencies greater than 20 kHz. However, frequencies exceeding 60 kHz in railway tracks tend to favor surface waves, making it challenging to detect internal cracks. To ensure the evaluation method's applicability across the entire cross-section of railway tracks while considering both detection accuracy and signal analysis complexity, this paper limits the frequency range to between 20 kHz and 60 kHz.

The detection of cracks in railway tracks using ultrasonic guided waves involves analyzing the echo signals generated by the interaction of cracks with guided wave modes to achieve crack localization. Since the same crack affects different modes to varying degrees, this paper employs modal crack zone energy and modal crack reflection intensity as evaluation indicators for the sensitivity of guided wave modes to cracks. The crack sensitivity, represented by C_s , reflects the material's propensity for crack initiation and growth under various conditions, as shown in Eq. (1):

$$C_s = G_c + Q_c \quad (1)$$

where G_c represents the energy within the modal crack zone, and Q_c indicates the number of evaluation indicators for the mechanism of modal crack reflection intensity.

2.1. Evaluation indicator for modal crack zone energy

Research indicates that ultrasonic guided waves applied for detecting cracks in specific locations of railway tracks show higher sensitivity to the crack when guided wave modes exhibit more pronounced vibrations at the crack location. It is common practice to select modes with larger amplitudes at the crack location and smaller amplitudes at other locations for detection. In this paper, we introduce the evaluation indicator G_c , which signifies the energy of the modal crack zone, to describe the vibrations of various modes near the crack site. The rail section is segmented into 250 units and 170 nodes, as shown in Fig. 1(a):

Assuming the coordinates of the two endpoints of the crack are denoted as $P_A(x_A, y_A)$ and $P_B(x_B, y_B)$, based on Eq. (2), determine the two nodes $P_{A'}(x_{A'}, y_{A'})$ and $P_{B'}(x_{B'}, y_{B'})$ on the cross-section that are closest to the crack endpoints. In this context, N_i signifies the total number of nodes on the rail section.

$$\begin{aligned} (x_{A'}, y_{A'}) &\propto \min \left(\sqrt{(x_{N_i} - x_A)^2 + (y_{N_i} - y_A)^2} \right), N_i \in [1, N] \\ (x_{B'}, y_{B'}) &\propto \min \left(\sqrt{(x_{N_i} - x_B)^2 + (y_{N_i} - y_B)^2} \right), N_i \in [1, N] \end{aligned} \quad (2)$$

Using the midpoint between $P_{A'}$ and $P_{B'}$ as $P_{C'}(x_{C'}, y_{C'})$, form a circle with $P_{C'}$ as the center and r as the radius. As illustrated in Fig. 1(b), the area of the rail section enclosed by the circle represents the designated crack zone, and the N nodes within this circle are selected to represent the energy magnitude of the crack zone. The node numbers are labeled as N_1, N_2, \dots, N . Where

$$x_{C'} = \frac{x_{A'} + x_{B'}}{2}, y_{C'} = \frac{y_{A'} + y_{B'}}{2}, r = \sqrt{(x_{A'} - x_{B'})^2 + (y_{A'} - y_{B'})^2} \quad (3)$$

According to the railway wave equation [23], calculate the vibrational mode data for all nodes in each direction for each mode, denoted as $V_x(f_i, N_i, m_i)$, $V_y(f_i, N_i, m_i)$ and $V_z(f_i, N_i, m_i)$ respectively. Here, f_i stands for the frequency, m_i is the mode index

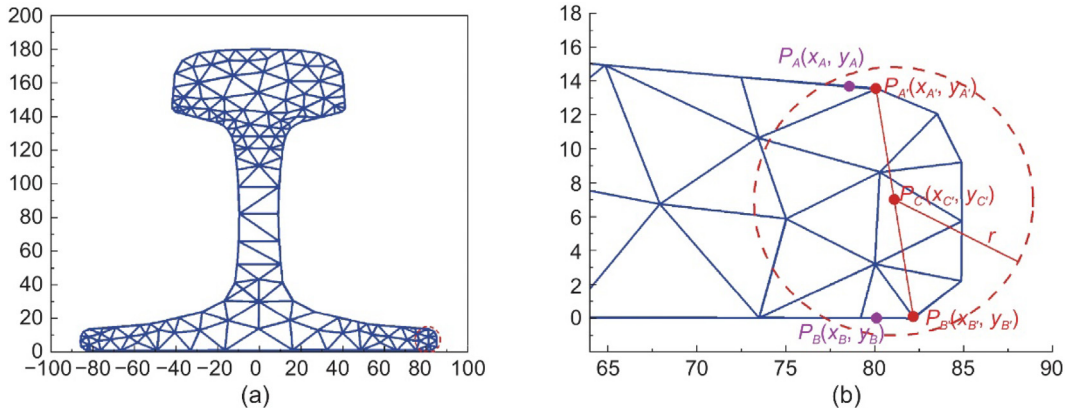


Fig. 1. Rail Cross-Section Mesh Division and Node Selection.

corresponding to frequency f_i , and N_i denotes the node index. Then, for each mode, the average vibrational displacement of the nodes near the crack and all nodes on the cross-section is given by:

$$V_c(f_i) = \frac{\sum_{N_1}^{N_c} \sqrt{V_x(f_i, N_i, m_i)^2 + V_y(f_i, N_i, m_i)^2 + V_z(f_i, N_i, m_i)^2}}{N_c} \quad (4)$$

$$V_a(f_i) = \frac{\sum_{N_1}^{N_a} \sqrt{V_x(f_i, N_i, m_i)^2 + V_y(f_i, N_i, m_i)^2 + V_z(f_i, N_i, m_i)^2}}{N_a}$$

where $N_i = N_1, N_2, \dots, N$, and the corresponding modal zone energy is represented by Eq. (5). This equation is used to characterize the vibration and energy distribution states of each mode near the crack zone.

$$G_c(f_i) = \frac{V_c(f_i) - V_a(f_i)}{V_c(f_i)} \quad (5)$$

When the average vibrational displacement of nodes in the crack zone is significantly smaller than the average vibrational displacement of all nodes on the rail section (i.e., $V_c(f_i) < V_a(f_i)$), $G_c(f_i) < 0$. Conversely, when the average vibrational displacement of nodes in the crack zone is much larger than the average vibrational displacement of all nodes on the rail section (i.e., $V_c(f_i) \gg V_a(f_i)$), $G_c(f_i)$ approaches 1. Normalize the results of Eq. (5) to obtain $G_c(f_i) \in [0, 1]$. From Eq. (5), it can be observed that when the coefficient $G_c(f_i)$ of the modal crack zone energy indicator is larger, the vibration of the mode in the crack zone is greater, indicating higher sensitivity to the crack. When $G_c(f_i)$ approaches 1, it signifies that the energy of the mode in the crack zone is significantly greater than the energy at other locations.

2.2. Evaluation indicator for modal crack reflection intensity

In railway crack detection, the detection results can be influenced by the collection equipment and on-site noise during the signal acquisition process. Low amplitude of the received crack echo signal can lead to a risk of false negatives. Therefore, modes with higher reflection echo amplitudes are more sensitive to cracks. When the vibration direction of the guided wave mode is orthogonal to the crack trend, the echo amplitude is greater than for modes with the vibration direction parallel to the crack trend. For modes where the vibration direction is neither orthogonal nor parallel to the crack trend, the amplitude falls between the two cases. Drawing on the vibration characteristics of the modes, this paper introduces the evaluation indicator Q_c to measure the intensity of modal crack reflection. At frequency f_i , the coefficient

for the crack reflection intensity of mode $Q_c(f_i)$ is determined by the following formula:

$$Q_c(f_i) = 1 - |Q \cdot P| \quad (6)$$

Here, Q denotes the mode vibration direction vector, and P represents the crack trend direction vector. When the crack direction is orthogonal to the mode vibration direction, $|Q \cdot P| = 0$ and $Q_c(f_i) = 1$. When the crack direction is parallel to the mode vibration direction, $|Q \cdot P|$ reaches its maximum, and $Q_c(f_i)$ reaches its minimum. Thus, as $Q_c(f_i)$ approaches 1, the orthogonality between the two improves, making the reflection wave from the crack more pronounced. To prevent abrupt changes in the calculation results, additional nodes must be incorporated into the vector. Using the finite element discretization method, the vibrational mode V at any point within a discretized element can be expressed using shape functions:

$$V^{(e)}(x, y, z, t) = \begin{bmatrix} \sum_{i=1}^n N_i(x, y) V_{xi} \\ \sum_{i=1}^n N_i(x, y) V_{yi} \\ \sum_{i=1}^n N_i(x, y) V_{zi} \end{bmatrix}^{(e)} e^{j(\xi z - \omega t)} = N(x, y) q^{(e)} e^{j(\xi z - \omega t)} \quad (7)$$

In the equation, $N(x, y)$ denotes the shape function matrix, $q^{(e)}$ represents the vibrational vector of the nodes, N_i denotes the shape functions of the finite element unit.

$$N(x, y) = \begin{bmatrix} N_1 & N_2 & \dots & N_n \\ N_1 & N_2 & \dots & N_n \\ N_1 & N_2 & \dots & N_n \end{bmatrix} \quad (8)$$

$$q^{(e)} = [V_{x1} \quad V_{y1} \quad V_{z1} \quad V_{x2} \quad V_{y2} \quad V_{z2} \quad \dots \quad V_{xn} \quad V_{yn} \quad V_{zn}]^T \quad (9)$$

At a frequency of f_i , the vibrational mode m_i at points $P_{A'}(x_{A'}, y_{A'})$ and $P_{B'}(x_{B'}, y_{B'})$ is represented as $V_{A'}$ and $V_{B'}$ respectively. Divide the line segment between $P_{A'}$ and $P_{B'}$ into four equal parts, labeling the three intermediate points as $P_{A'_1}(x_{A'_1}, y_{A'_1})$, $P_{A'_2}(x_{A'_2}, y_{A'_2})$, $P_{A'_3}(x_{A'_3}, y_{A'_3})$. Using the vibrational data from the three nodes in the triangular element where these intermediate points are located, Eqs. (7), (8), and (9) can be applied to determine the

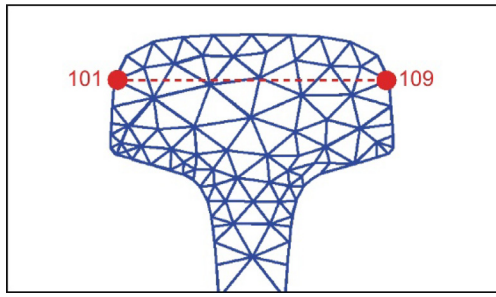


Fig. 2. Transverse Crack in Rail Head.

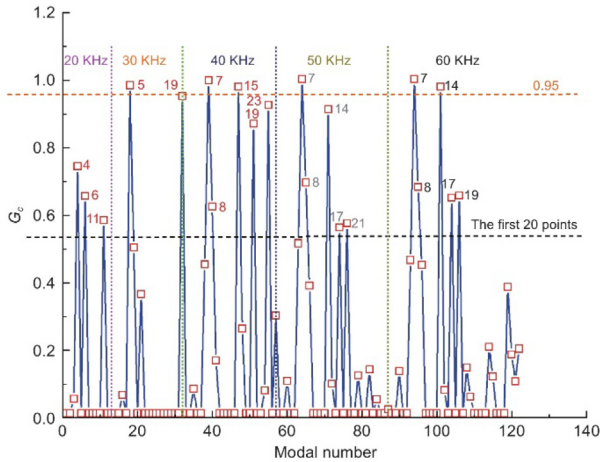


Fig. 3. Calculation Results of Modal Crack Zone Energy Indicator G_c .

Table 1

Evaluated values of crack reflection intensity Q_c for transverse cracks in the rail head.

Frequency (KHz)	Modal number	Q_c
3	5	0.751
	17	0.191
4	7	0.314
	14	0.961
5	6	0.492
6	7	0.612
	13	0.212

Table 2

Sensitivity parameters of modes.

Frequency (KHz)	Modal number	G_c	Q_c
4	7	1.000	0.313
5	1	0.000	1.000
6	7	1.000	0.611

vibrational data $V_{A'_1}, V_{A'_2}, V_{A'_3}$ at these three intermediate points. This, together with $V_{A'}$ and $V_{B'}$, forms a new vibrational vector denoted as Q :

$$Q = [V_{A'}, V_{A'_1}, V_{A'_2}, V_{A'_3}, V_{B'}] \quad (10)$$

Similarly, divide the line segment between the crack points P_A and P_B into four equal parts, labeling the three intermediate points as $P_{A_1}(x_{A_1}, y_{A_1}), P_{A_2}(x_{A_2}, y_{A_2}), P_{A_3}(x_{A_3}, y_{A_3})$. Together with points P_A and P_B , this forms a coordinate vector denoted as P :

$$P = [A, A_1, A_2, A_3, B]^T \quad (11)$$

If the mode vibration direction is orthogonal to the crack trend, $|Q \cdot P| = 0, Q_c(f_i) = 1$, and if the mode vibration direction is not orthogonal, $|Q \cdot P| > 0, Q_c(f_i) < 1$. Normalize the results of Eq. (6) to obtain $Q_c(f_i) \in [0, 1]$. Therefore, as the coefficient of the modal crack reflection intensity evaluation indicator approaches 1, the greater the orthogonality between the mode and the crack, the more pronounced the reflection when the mode encounters the crack.

In summary, the extent to which a crack affects guided wave modes correlates positively with the magnitude of the modal crack zone energy evaluation indicator. When the energy within the crack zone is relatively consistent, a higher crack reflection intensity results in greater echo amplitudes, indicating a heightened sensitivity of the mode to the crack.

3. Simulation analysis and experimental validation

To validate the influence of the crack zone energy evaluation indicator and the crack reflection intensity evaluation indicator on guided wave modes, this study focuses on validating the algorithm using transverse cracks in rail heads as the research subject. Considering crack detection accuracy, guided wave coverage, and detection complexity, the research frequency range is defined within 20 kHz–60 kHz.

3.1. Simulation analysis

The positions of transverse cracks in the rail head are illustrated in Fig. 2.

In this study, we assume points P_A and P_B coincide with points $P_{A'}$ and $P_{B'}$, located at nodes 101 and 109 on the cross-section. The longitudinal coordinates of the crack's endpoints are set to zero. Five frequency points are selected from the specified range: 20 kHz, 30 kHz, 40 kHz, 50 kHz, and 60 kHz. Using the wave equation for the rail, we calculate the vibrational data for all modes at these frequencies, totaling 123 modes. Applying Equation (5), we determine the crack zone energy evaluation indicator G_c for all modes, as shown in Fig. 3.

Based on the calculated modal crack zone energy for transverse cracks in the rail head, the modes corresponding to G_c are selected. For each of these modes, the crack reflection intensity evaluation indicator Q_c is computed. The values are then sorted in descending order, and the results are displayed in Table 1.

From Table 1, it is evident that the crack reflection intensity evaluation indicator Q_c varies across different modes, even when the crack zone energy evaluation indicator G_c for transverse cracks in the rail head is equal to 1. Notably, the reflection intensity for mode 7 at 60 kHz is about twice that of mode 7 at 40 kHz. Among the 123 modes, transverse cracks in the rail head significantly impact mode 14 at 40 kHz, mode 5 at 30 kHz, mode 7 between 40 kHz and 60 kHz, mode 13 at 60 kHz, and mode 17 at 30 kHz.

For mode 7 at 60 kHz, which exhibits the highest crack zone energy indicator G_c , a comparison is made with mode 7 at 40 kHz, where the crack reflection intensity G_c is equivalent but differs by a factor of two. Similarly, to analyze the impact of the crack zone energy indicator G on the mode selection results and the relative influence of G_c and Q_c , mode 1 at 50 kHz, which has a G_c value of 0 but the highest Q_c value, is selected for comparison and validation. The crack zone energy evaluation indicators and reflection intensity evaluation indicator coefficients for these three modes are shown in Table 2.

According to the configuration specified by $L_{grid} \leq \lambda \min / 10$, the grid width along the rail's length is set to 3 mm, with the crack positioned at 1.73 m. An excitation point is located at the

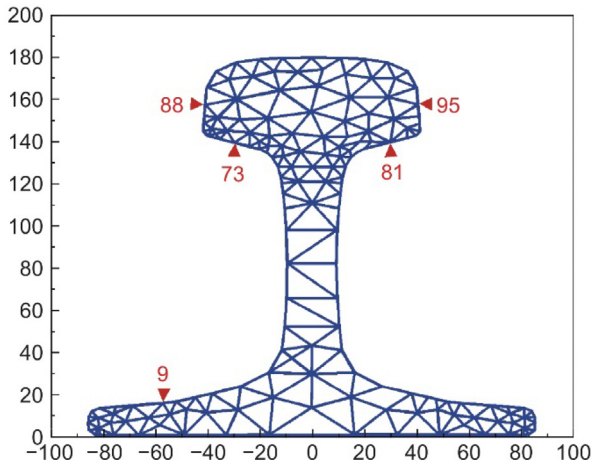


Fig. 4. Excitation and Reception Node Locations.

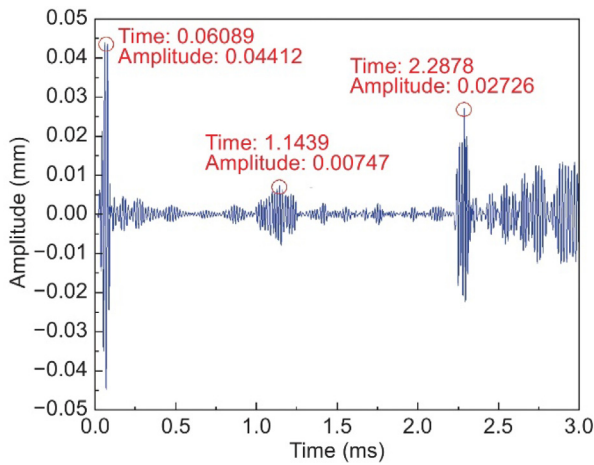


Fig. 5. Simulation results for mode 7 at a frequency of 60 kHz.

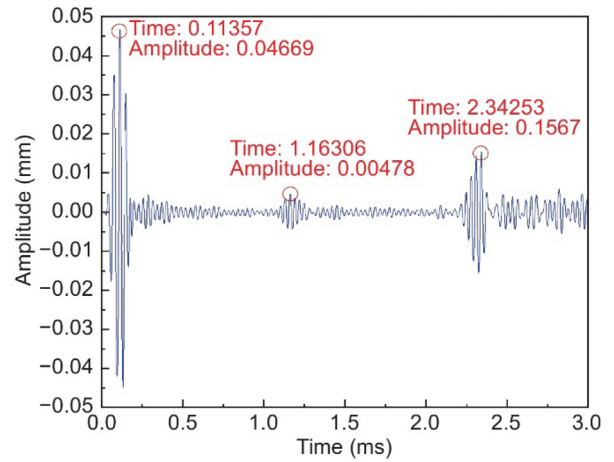


Fig. 6. Depicts the simulation results for mode 7 at a frequency of 40 kHz over the time interval from 0 to 3 ms.

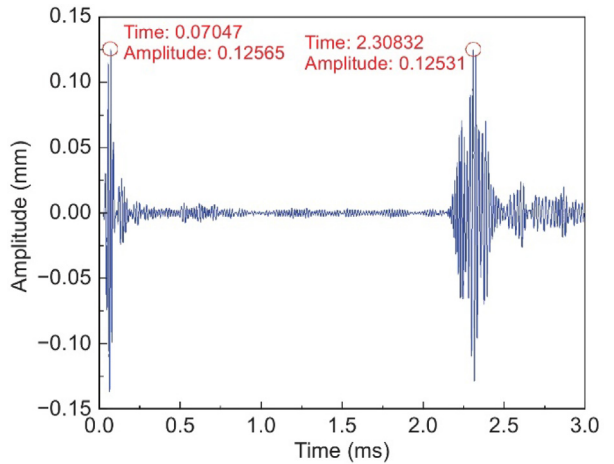


Fig. 7. Simulation results for mode 1 at a frequency of 50 kHz.

rail's end at 0 m, using a sinusoidal wave modulated by a 5-cycle Hanning window as the excitation signal, with a central frequency of 60 kHz. A receiver is placed 60 mm away in the same direction, at the same node as the excitation point. For the 60 kHz frequency, the mode 7 is excited vertically at nodes 73 and 81, and the signal is received at node 81. For the 40 kHz frequency, the 7th mode is excited vertically at nodes 88 and 95, with the signal received at node 95. For the 50 kHz frequency, the mode 1 is both excited and received at node 9. The positions of these nodes are shown in Fig. 4.

The calculations were performed using the three-dimensional finite element simulation software ANSYS. The simulation ran for a total duration of 3 ms, divided into 3600 calculation steps. The results of the simulation are shown in Fig. 5, which shows the received and reflected waveforms (marked in the figure) of Mode 7 at a frequency of 60 kHz. The first waveform corresponds to the direct wave received, the second waveform corresponds to the reflection from the rail bottom crack, and the third waveform corresponds to the reflection from the rail end face. The distance between the end face and the receiving position is $d = 3.43$ m. The peak time of the direct wave packet, denoted as t_0 , is 0.06089 ms. The peak time of the rail crack echo wave packet, denoted as t_1 , is 1.1439 ms, with an amplitude of 0.00713 mm. The peak time of the end face echo wave packet, denoted as t_2 , is 2.2878 ms.

Fig. 6 displays the received and reflected waveforms (marked in the figure) of Mode 7 at a frequency of 40 kHz. In the signal, the first waveform corresponds to the direct wave received, the second waveform corresponds to the reflection from the rail bottom crack, and the third waveform corresponds to the reflection from the rail end face. The distance between the end face and the receiving position is $d = 3.43$ m. The peak time of the direct wave packet, denoted as t_0 , is 0.04669 ms. The peak time of the rail crack echo wave packet, denoted as t_1 , is 1.16306 ms, with an amplitude of 0.00478 mm. The peak time of the end face echo wave packet, denoted as t_2 , is 2.34253 ms.

Fig. 7 illustrates the received and reflected waveforms of Mode 1 at a frequency of 60 kHz. In the signal, the first waveform corresponds to the direct wave received, and there are no reflections for Mode 1. The third waveform corresponds to the reflection from the rail end face. The distance between the end face and the receiving position is $d = 3.45$ m. The peak time of the direct wave packet, denoted as t_0 , is 0.07047 ms. The peak time of the end face echo wave packet, denoted as t_2 , is 2.30832 ms.

Based on Eq. (12), the group velocity of Mode 7 at 60 kHz is calculated as $V_{mg} = 3138.6$ m/s, which differs from the theoretical group velocity of $V_{mg,t} = 3154.2$ m/s by only 15.6 m/s. This difference falls within an acceptable range of error. Therefore, the excited mode is confirmed to be Mode 7. Using the received crack echo signal, Eq. (13) is utilized to calculate the crack position

d_0 , where $V_{mg,t}$ represents the theoretical group velocity of the mode.

$$V_{mg} = \frac{2 \times d}{t_2 - t_0} \quad (12)$$

$$d_0 = 0.06 + \frac{(t_1 - t_0) \times V_{mg,t}}{2} \quad (13)$$

The simulation calculation results for the crack position indicate a location of 1.72 m along the rail, with only a 0.02 m deviation from the actual crack position of 1.75 m. Hence, it can be concluded that Mode 7 can detect transverse cracks on the rail head. Analysis of the data reveals the successful induction of Mode 7 and Mode 1 through the excitation method. In Fig. 6, the received signal of Mode 7 at 40 kHz frequency exhibits a crack echo, facilitating the detection of transverse cracks on the rail head with a deviation of only 0.1 m. However, the amplitude of the crack echo is 36.74% lower compared to Mode 7 at 60 kHz frequency. Conversely, the received signal of Mode 1 at 50 kHz frequency in Fig. 7 does not demonstrate a crack echo, indicating an inability to detect transverse cracks on the rail head.

Therefore, among the three modes, Mode 7 at 60 kHz frequency is most sensitive to transverse cracks on the rail head, showing superior crack detection performance. Following closely, Mode 7 at 40 kHz frequency, with a higher crack zone energy evaluation indicator, also displays good crack detection capability. Conversely, Mode 1 at 50 kHz frequency exhibits minimal sensitivity to transverse cracks, thereby failing to detect cracks on the rail head, which aligns with the calculated results of crack influence on guided wave modes.

3.2. Experimental validation

During the experiment, the side of the rail was deliberately broken. With a length of 3.5 m, the crack is precisely located at 1.685 meters along the rail. To explore the influence of cracks on guided wave modes, we have excited the rail with Mode 7 at a frequency of 60 kHz and Mode 1 at a frequency of 50 kHz. To excite Mode 7, two transducers with a central frequency of 60 kHz are vertically affixed at nodes 81 and 89 of the rail head at one end of the rail. They are oriented in the same direction for excitation, with receiving transducers positioned 0.05 meters from the end face. The excitation signal, generated by a signal generator and amplified, is a sinusoidal wave modulated with a Hanning window, spanning 5 cycles at a frequency of 60 kHz.

The crack detection experiment for Mode 7 was conducted in a total of 10 sets. The received signals were collected using an oscilloscope, and the results were averaged. The processed results are depicted in Fig. 8. In Fig. 8, clear reflections of the crack (marked as the second indicator) and signals from the rail head end (marked as the third indicator) are evident. By computing the time difference between the peak of the crack reflection signal and the direct wave signal, and concurrently deriving the theoretical group velocity of Mode 7, the distance between the crack and the receiving transducer can be determined using Eq. (13). The calculated distance is 1.708 m, with only a 0.023-meter deviation from the actual distance of 1.685 m. Hence, this mode is capable of detecting cracks on the rail head, aligning with the outcomes of simulation analyses.

To excite Mode 1, transducers with a central frequency of 50 kHz were affixed at node 11 on one end of the rail, with receiving transducers positioned at node 11, 0.05 meters away. The excitation signal, a sinusoidal wave modulated with a Hanning window spanning 5 cycles at a frequency of 50 kHz, was generated by a signal generator and amplified before being applied to the rail. Similarly, 10 sets of received signals were collected and averaged. The results are shown in Fig. 9, which can be observed

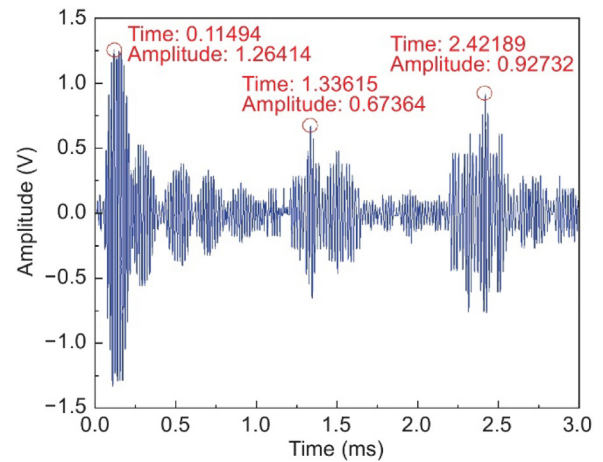


Fig. 8. Experimental Results of 7th Mode at 60 kHz.

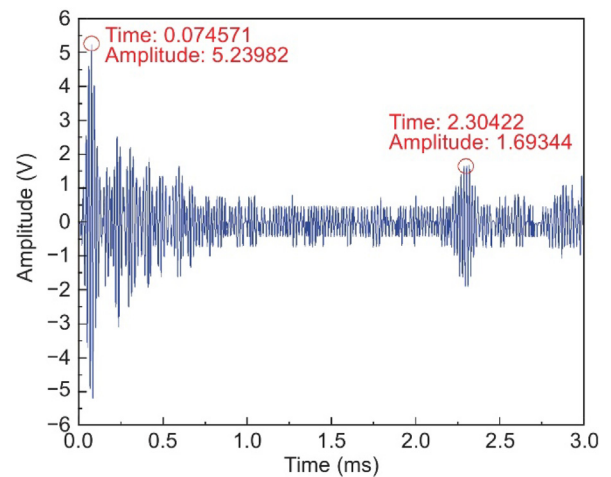


Fig. 9. Experimental Results for the 1st Mode at 50 kHz.

that only one end-face echo signal is present in the waveform (marked as the second indicator), with no crack reflection signal detected. Consequently, the influence of cracks on Mode 1 is minimal, indicating that Mode 1 cannot detect rail head cracks. This result is consistent with the simulation findings. The comprehensive analysis of simulation and experimental validation results reveals that the modal crack zone energy evaluation index predominantly influences the effect of cracks on modes, playing a decisive role, while the modal crack reflection intensity evaluation index assumes a secondary position, serving as a screening criterion. In practical applications, the evaluation index S_{re} is initially computed to select modes within $S_{re} \in [0.95, 1]$, followed by the calculation of their evaluation index S_{ri} , and selecting modes with higher S_{ri} values as the detection modes for the crack. Through simulation and experimental analyses, it is evident that the proposed method for selecting the optimal detection mode for rail cracks based on modal crack sensitivity of guided waves is effective.

4. Conclusion

In pursuit of selecting the most effective detection modes for various types of cracks, the paper presents a methodology grounded in guided wave mode crack sensitivity evaluation. By establishing metrics for crack area energy and reflection intensity,

contingent upon the location and directional trend of crack propagation, the study delves into the mechanics of crack influence on guided wave modes. This facilitates the identification of the optimal detection mode for rail head cracks. Segmenting the rail cross-section into seven distinct regions, the paper then selects detection modes tailored to prevalent crack types across the entire cross-sectional area. Simulation and experimental findings validate the accuracy of guided wave modes identified through this approach, thereby establishing a foundational framework for the exploration of crack detection and localization methods spanning the entirety of rail cross-sections. This method can provide important technical support for robotic real-time rail crack detection.

CRedit authorship contribution statement

Jianjun Liu: Resources, Data curation, Conceptualization. **Huan Luo:** Writing – original draft, Funding acquisition. **Han Hu:** Writing – original draft, Methodology. **Jian Li:** Resources, Funding acquisition.

Declaration of competing interest

The authors declare that they have no known competing financial interests or personal relationships that could have appeared to influence the work reported in this paper.

Acknowledgments

This work is supported by Natural Science Foundation of Guangdong Province, China (2022A1515011409 and 2023A1515011253); supported by Key Areas Special Project of General Universities in Guangdong Province, China (2023ZDZX1024); supported in part by research grants from The Youth Project of National Natural Science Foundation of China (52105268); supported in part by the Key Project of Shaoguan University, China (SZ2020KJ02); supported in part by Youth Project of National Natural Science Foundation of China (62001200), supported in part by the Natural Science Foundation of Fujian Province, China (2020J01817); supported by Shaoguan Social Development Science and Technology Collaborative Innovation System Construction Project, China (230330178036242 and 230330098033679); supported in part by Shaoguan University Ph.D. Initiation Project: Research on the Consistency Problem of Nonlinear Multi-agent Systems, China (440-9900064604); supported in part by 2024 Key Scientific Research Project of Shaoguan University: Research on Autonomous Exploration System of Rescue Robot, China; supported in part by the Higher education institution featured innovation project of Department of Education of Guangdong Province, China (2023KTSCX138); supported in part by the Natural Science Foundation of Chongqing, China (CSTB2022NSCQMSX1386); supported in part by Shaoguan University Ph.D. Initiation Project, China (440-9900064602); supported in part by Guangdong Province Key Construction Discipline Research Capacity Enhancement Project (2022ZDJS051, 2021ZDJS070).

References

- [1] W. Zeng, Y.Z. Liu, S.Z. Yu, S.K. Qi, H. Wu, L. Liu, Research on ultrasonic guided wave technology for the rail fatigue cracks based on PCA-adaboost. M2 Algorithm, *J. Test. Eval.* 52 (1) (2024) 545–556.
- [2] H.P. Chen, G.Y. Zhang, et al., Nondestructive determination of longitudinal rail stress from guided wave dispersion properties, *Constr. Build. Technol.* 408 (2023) 133618.
- [3] F. Deng, S.Q. Li, X.R. Zhang, L. Zhao, J.B. Huang, C. Zhou, An intelligence method for recognizing multiple defects in rail, *Sensors* 21 (23) (2021) 8108.
- [4] P. Rizzo, E. Sorrivi, F.L. di Scalea, E. Viola, Wavelet-based outlier analysis for guided wave structural monitoring: Application to multi-wire strands, *J. Sound Vib.* 307 (1–2) (2002) 52–68.
- [5] J.P. Jiao, B. Wu, C.F. He, R.Y. Fei, Y. Li, Experimental research on guided waves propagation in thin plate using wavelet transform and mode acoustic emission, *China Mech. Eng.* (13) (2004) 51–54.
- [6] S.H.M. Rizvi, M. Abbas, An advanced Wigner-Ville time-frequency analysis of Lamb wave signals based upon an autoregressive model for efficient damage inspection, *Meas. Sci. Technol.* 32 (9) (2021) 095601.
- [7] J.H. Wu, X.L. Chen, Z.S. Ma, A signal decomposition method for ultrasonic guided wave generated from debonding combining smoothed pseudo Wigner-Ville distribution and vold-Kalman filter order tracking, *Shock Vib.* 2017 (2017) 7283450.
- [8] W.H. Prosser, M.D. Seale, B.T. Smith, Time-frequency analysis of the dispersion of Lamb modes, *J. Acoust. Soc. Am.* 105 (5) (1999) 2669–2676.
- [9] T.A. De-an, LIU. Zhen-qing, Two-dimensional fast Fourier transform and Wigner-Ville transform in ultrasonic nondestructive testing, *DNT* (07) (2001) 313–316.
- [10] C.F. He, Y. Li, X.Y. Wang, et al., Ultrasonic guided wave signal analysis based on wavelet transform and Wigner-Ville transform, *Exp. Mech.* (04) (2005) 584–588.
- [11] X.U. Zhenying, L.L.U. Huan, W.A.N. Dongyan, Hong HONG, Signal analysis method for weld feature-guided wave based on Wigner-Ville distribution, *China Meas. Test* 43 (09) (2017) 29–34.
- [12] D. Alleyne, P. Cawley, A two-dimensional Fourier transform method for the measurement of propagating multimode signals, *J. Acoust. Soc. Am.* 89 (3) (1991) 1159–1168.
- [13] D. Alleyne, P. Cawley, A 2-dimensional Fourier transform method for the quantitative measurement of Lamb modes, *Ultrason. Symp.* (1990) 1143–1146.
- [14] S. Fateri, N.V. Boulgouris, A. Wilkinson, A two-dimensional fast Fourier transform using incremented frequency measurement for guided wave analysis, *Insight* 56 (9) (2014) 499–504.
- [15] X.L. Deán-Ben, C. Trillo, A.F. Doval, J.L. Fernández, Characterization of guided acoustic waves in an arbitrary direction with full-field instantaneous maps of the acoustic displacement, *J. Appl. Phys.* 112 (4) (2012) 044504.
- [16] Y.H. Da, G.R. Dong, B. Wang, D.Z. Liu, Z.H. Qian, A novel approach to surface defect detection, *Int. J. Eng. Sci.* 133 (2018) 181–195.
- [17] K.A. Tiwari, R. Raisutis, V. Samaitis, Hybrid signal processing technique to improve the defect estimation in ultrasonic non-destructive testing of composite structures, *Sensors* 17 (12) (2017) 2858.
- [18] F.Y. Teng, J.T. Wei, S.S. Lv, X.Y. Geng, C. Peng, L. Zhang, Z.Y. Ju, L. Jia, M.S. Jiang, Damage localization in carbon fiber composite plate combining ultrasonic guided wave instantaneous energy characteristics and probabilistic imaging method, *Measurement* 221 (2023) 113443.
- [19] S. Gharehdash, M. Laleh, D. Sainsbury, M. Barzegar, B.A. Sainsbury, Low-frequency ultrasonic tomography of corrosion-induced damage patterns on naturally corroded solid reinforcing bar rock bolts, *Constr. Build. Mater.* 392 (2023) 131694.
- [20] P.W. Loveday, C.S. Long, Modal amplitude extraction of guided waves in rails using scanning laser vibrometer measurements, in: *Review of Progress in Quantitative Nondestructive Evaluation AIP Conf. 2012*, American Institute of Physics, 2012, pp. 182–189, 1430.
- [21] P.W. Loveday, C.S. Long, Field measurement of guided wave modes in rail track, in: *The 39th Annual Review of Progress in Quantitative Nondestructive Evaluation AIP Conf. 2013*, American Institute of Physics, 2013, pp. 230–237, 1511.
- [22] P.W. Loveday, C.S. Long, Laser vibrometer measurement of guided wave modes in rail track, *Ultrasonics* 57 (2015) 209–217.
- [23] D.N. Alleyne, P. Cawley, Optimization of Lamb wave inspection techniques, *NDT & E Int.* 25 (1) (1992) 11–22.
- [24] F.L. Degertekin, B.T. Khuri-Yakub, Single mode Lamb wave excitation in thin plates by Hertzian contacts, *Appl. Phys.* 69 (2) (1996) 146–148.
- [25] U. Amjad, S.K. Yadav, T. Kundu, Detection and quantification of diameter reduction due to corrosion in reinforcing steel bars, *Struct. Health Monit.* 14 (5) (2015) 532–543.
- [26] M.S. Prasad, V.R. Kumar, K. Balasubramaniam, et al., Imaging of defects in composite structures using guided ultrasonics, *Proc. SPIE - Int. Soc. Opt. Eng.* 5062 (2003) 700–703.
- [27] Z.G. Zhou, Z.Y. Feng, Y.F. Gao, X. Zhu, Application of time frequency analysis to ultrasonic-guided-wave signal interpretation, *J. Beijing Univ. Aeronaut. Astronaut.* 34 (7) (2008) 833–837.
- [28] Z.Y. Feng, Basic Research on Ultrasonic Guided Wave Testing Technology for Bonding Quality of Aluminum Clad Honeycomb Plate, *Beijing University of Aeronautics and Astronautics*, Beijing, 2016, pp. 20–97.
- [29] F.L.D. Scalea, J. Mcnamara, Ultrasonic NDE of railroad tracks: Air-coupled cross-sectional inspection and long-range inspection, *Or Insight* 45 (6) (2003) 394–401.

- [30] D.S.F. Lanza, J.D. Mcnamara, Measuring high-frequency wave propagation in railroad tracks by joint time-frequency analysis, *J. Sound Vib.* 273 (3) (2004) 637–651.
- [31] J.D. Mcnamara, Health Monitoring of Railroad Tracks by Elastic-Wave Based Non-Destructive Testing, University of California, San Diego, 2003, pp. 21–95.
- [32] I. Bartoli, F.L.D. Scalea, M. Fateh, et al., Modeling guided wave propagation with application to the long-range defect detection in railroad tracks, *Ndt & E Int.* 38 (5) (2005) 325–334.
- [33] L.U. Chao, Rui chen LIU, Jun jie CHANG, Guided waves dispersion curves and wave structures of the rail's vertically vibrating, *J. Vib. Eng.* 27 (04) (2014) 598–604.
- [34] Z.-Q. Liu, T.A. De-an, Mode identify of Lamb wave by means of 2-D FFT, *Acoust. Technol.* (04) (2000) 212–214+219.
- [35] J. Wang, Research on Temperature Stress Estimation Algorithm of Seamless Rail Based on Guided Wave Multimodal Fusion, Beijing Jiaotong University, Beijing, 2018, pp. 25–118.
- [36] B. Xing, Z. Yu, X. Xu, et al., Research on a rail defect location method based on a single mode extraction algorithm, *Appl. Sci.* 9 (6) (2019) 1–16.